Sensors & Actuators: B. Chemical 401 (2024) 134948

Contents lists available at ScienceDirect

Sensors and Actuators: B. Chemical

journal homepage: www.elsevier.com/locate/snb

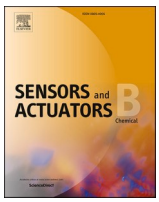

Self-referenced dual-near-infrared emission-based sensor platform for the ultrasensitive discrimination of D_2O and H_2O

Dongkyu Kang [a,1], Eunjin Park [a,1], Kayoung Kim [b], Joonseok Lee [a,c,d,*]

[a] Department of Chemistry, Hanyang University, Seoul 04763, Republic of Korea
[b] Department of Fiber Convergence Material Engineering, Dankook University, Gyeonggi-do 16890, Republic of Korea
[c] Research Institute for Convergence of Basic Sciences, Hanyang University, Seoul 04763, Republic of Korea
[d] Research Institute for Natural Sciences, Hanyang University, Seoul 04763, Republic of Korea

ARTICLE INFO

Keywords:
Discriminations of D_2O and H_2O
Dual-Near-infrared signal
Lanthanide-doped nanoparticles
Self-reference

ABSTRACT

Due to its chemical and physical similarities, the ultrasensitive discrimination of D_2O in the presence of H_2O remains a practical challenge. In this study, we present an approach to utilize the near-infrared (NIR) optical properties of H_2O. Specifically, the absorption coefficient of H_2O at approximately 980 nm, which is derived from the second overtone of the O–H stretching mode of H_2O, exhibits a notable distinction from that of D_2O. To this end, we construct and optimize a dual-NIR emissive lanthanide-doped nanoprobe with a strong emission intensity at 980 nm. In addition, to enhance the reliability of the proposed sensor platform, we introduce a self-referenced signal at 865 nm, which shows a stable signal intensity in both H_2O and D_2O. Our self-referenced dual-NIR emission-based sensor platform successfully discriminates between D_2O and H_2O and shows ultrasensitive discrimination capabilities with a limit of detection of 0.17 nM, which has the highest sensitivity among that of previously reported D_2O sensors.

1. Introduction

Heavy water (D_2O) is an isotopic species of H_2O and has significant implications for various fields, including chemical reactions, nuclear reactors, and biological analysis [1,2]. The purity of D_2O, a crucial factor, must be considered in all these applications because its impurities can affect the rate and yield of chemical reactions and alter the properties of the final products [3]. However, discriminating between D_2O and H_2O remains an ongoing challenge because D_2O is highly hygroscopic, and its chemical and physical properties are very similar to those of H_2O [4]. Traditional methods for the discrimination of D_2O, including nuclear magnetic resonance and Fourier transform infrared (FT-IR), are widely available. However, these methods often require expensive equipment, are time-consuming, and may suffer from relatively sophisticated operation processes [5].

Optical sensors have emerged as a promising alternative method for D_2O detection owing to their various advantages, such as rapid and user-friendly processes [1,2,6–8]. Previous research has demonstrated that luminescence quenching originates from the high-energy vibrations of solvent molecules. In particular, solvents containing a hydroxyl group (with an O–H vibration frequency of approximately 3500 cm^{-1}) can elevate the vibrational relaxation rate, thereby resulting in a reduction in luminescence intensities. However, when the oxygen of the hydroxyl group is replaced by deuterium, the vibrational relaxation rate decreases because of the lower vibrational frequency of O–D (2550 cm^{-1}) compared with that of the O–H group [9,10]. Nonetheless, owing to the small difference in frequency, substantial challenges remain in quantifying D_2O in H_2O with high sensitivity.

In this study, we exploit the strong absorption coefficient of H_2O in the infrared region at a wavelength of 980 nm to distinguish between H_2O and D_2O. This phenomenon is attributed to the second overtone of the O–H stretching mode of H_2O ($\nu = 3$, $\varepsilon_{980} = 4{\cdot}10^{-3}$ $cm^{-1}M^{-1}$), whereas D_2O exhibits a negligible absorption coefficient ($\nu = 4$, $\varepsilon_{980} < 10^{-5}$ $cm^{-1}M^{-1}$). At this specific wavelength, there is a two-order of

Abbreviations: DHDNs, D_2O/H_2O discriminating nanoprobes; NIR, near-infrared; FT-IR, Fourier transform infrared; LOD, limit of detection; NP, nanoparticle; XRD, X-ray diffraction; PBS, Phosphate buffered saline; HEPES, 4-(2-hydroxyethyl)-1-piperazineethanesulfonic acid; RB, Rose bengal (4,5,6,7-tetrachloro-2′,4′,5′,7′-tetraiodofluorescein); MB, Methylene blue (Methylthioninium chloride).

* Corresponding author at: Department of Chemistry, Hanyang University, Seoul 04763, Republic of Korea.
E-mail address: joonseoklee@hanyang.ac.kr (J. Lee).

[1] These authors contributed equally.

https://doi.org/10.1016/j.snb.2023.134948
Received 22 September 2023; Received in revised form 23 October 2023; Accepted 6 November 2023
Available online 7 November 2023

magnitude difference in absorption coefficient at 980 nm between H_2O and D_2O.[11].

We present an approach for the ultrasensitive discrimination of D_2O and H_2O using the 980 nm-emission of lanthanide-doped nanoprobes (D_2O/H_2O discriminating nanoprobes, DHDNs) (Fig. 1). DHDNs were optimized to emit strong luminescence at 980 nm, which overlaps with the strong absorption of H_2O under 808 nm excitation, and a negligible absorption wavelength at 865 nm for both D_2O and H_2O [12,13]. To the best of our knowledge, this is the first report of a D_2O sensor platform that utilizes the near-infrared (NIR) optical properties of H_2O [2,14,15]. To ensure the reliability of the proposed sensor platform, we introduced an additional signal at 865 nm from the DHDN as a self-referenced signal. Because this is not perturbed by absorption in either D_2O or H_2O, this 865 nm-signal is an ideal reference signal for our D_2O sensor platform. Reference signals are essential in sensor applications because they precisely compensate for fluctuations in light intensity that may occur during the measurement process, including environmental conditions, noise, and light scattering [16,17]. This reference signal is called the ratio-metric approach, which relies on analyte-induced changes in two or more signals and greatly improves the quality of quantification [18–20]. Finally, the proposed sensor platform exhibited a remarkable discrimination capability with an ultralow limit of detection (LOD) of 0.17 nM, essentially surpassing the sensitivity of previously reported D_2O sensors. Therefore, we believe that our sensor platform has great potential in various fields where ultrasensitive discrimination of D_2O is required, such as in chemistry, physics, and biology.

2. Experimental

2.1. Materials

Neodymium (III) acetate hydrate (99.9 %), ytterbium (III) acetate hydrate (99.9 %), yttrium (III) acetate hydrate (99.9 %), neodymium (III) chlorides (99.9 %), oleic acid (OA, 90 %), 1-octadecene (ODE, 90 %), sodium hydroxide (NaOH, ≥ 98 %), ammonium fluoride (NH_4F, ≥ 99.9 %), ethanol (absolute), methanol (≥ 99.8 %), cyclohexane (≥ 99 %), tetrahydrofuran (THF, ≥ 99.9 %), dopamine hydrochloride (≥ 99.9 %), and hydrochloric acid (HCl, 37 %), Phosphate buffered saline (PBS), 4,5,6,7-tetrachloro-2′,4′,5′,7′-tetraiodofluorescein (Rose Bengal), Methylthioninium chloride (Methylene blue), Deuterium oxide (D_2O, 99.9 %) were purchased from Sigma-Aldrich, St. Louis, Mo, USA.

4-(2-hydroxyethyl)-1-piperazineethanesulfonic acid (HEPES, 1M) was purchased from ThermoFisher Scientific Inc, Waltham, MA, USA.

2.2. Synthesis of dual-NIR emissive D_2O/H_2O detecting nanoprobes

D_2O/H_2O discriminating nanoprobe (DHDN) was synthesized by the thermal decomposition method of lanthanide acetate precursors. In the general process of core DHDN's synthesis, $Ln(CH_3CO_2)_3$ (Ln = Y, Nd, or Yb total 0.4 mmol) was mixed with 3 mL of OA and 7 mL of ODE. The mixture was heated up to 150 °C, held for 1 h, and then cooled to 50 °C. Continuously, 5 mL of a methanolic solution of NaOH (1 mmol) and NH_4F (1.6 mmol) was added to the oleate–lanthanide solution and then stirred at 50 °C for 1 h. The obtained solution was subsequently heated to 100 °C and degassed through the vacuum pump for 1 h. Thereafter, the solution was heated to 300 °C and maintained under argon gas for 1 h. Finally, as-synthesized DHDN was cooled down to room temperature. The Final core DHDN was collected by centrifugation (3000 rpm) and washed 3times. The final product was re-dispersed in cyclohexane (2 mL) for the synthesis of the core@shell DHDN. The core@shell DHDN was synthesized following an identical procedure with a few modifications to the synthesis of core DHDN. $Ln(CH_3CO_2)_3$ (Ln = Y, total 0.2 mmol) $Ln(CH_3CO_2)_3$ (Ln=Y, total 0.2 mmol) were used in the synthesis of core@shell DHDN.

2.3. Water-solubilizations of DHDN

15 mg of the as-synthesized DHDN was dissolved in THF solution, while dopamine hydrochloride (50 mg) was dissolved in deionized water. Subsequently, these solutions were mixed in 7 mL of THF solution. Thereafter, the mixture is then placed in a 50 mL flask and heated at 50 °C with vigorous agitation under argon atmosphere for 5 h. 100 μL of 1 M HCl was added to the solution and the resultant NH_2-ligand DHDN was collected by centrifugation (10,000 rpm) and washed 3 times. Water-soluble DHDN was re-dispersed in water (1 mL) for D_2O sensing.

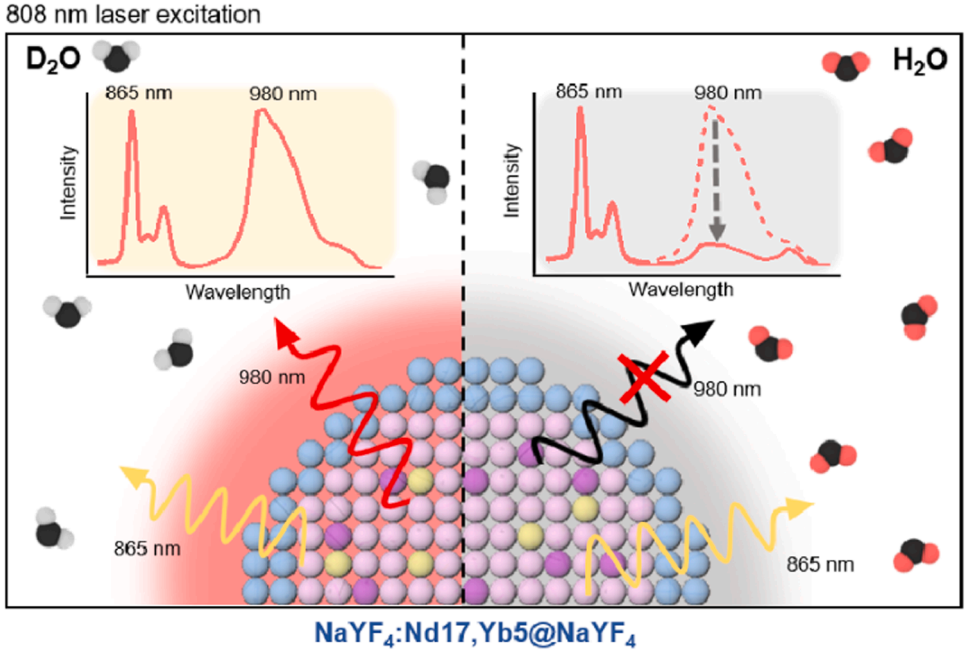

Fig. 1. Schematic illustrations of the developed D_2O/H_2O discriminating nanoprobe (DHDN) and their D_2O sensing process.

2.4. D_2O sensing using a lab-made portable sensing platform

Gradual dilutions of D_2O in H_2O solutions were prepared from 2.7 M to 0.55 nM. Then, 100 ug of DHDN was dispersed in a prepared D_2O/H_2O solution. The solution was then transferred to a 12.5 mm * 22.5 mm transparent quartz cuvette. Afterward, the cuvette was placed onto the lab-made portable detection platform. Thereafter, the discrimination of D_2O in H_2O was conducted by monitoring the 980 nm and 865 nm luminescence intensity using the USB NIR camera with a mobile device under excitation at 808 nm. The LOD of D_2O/H_2O was calculated from the calibration curve from the average of three independent tests. LOD was defined based on the equation $3.3\sigma/S$ where σ is the standard deviation and s is the slope of the calibration curve.

2.5. Characterizations

In this study, the UV–visible absorption spectra were recorded on the Cary 5000 UV-Vis-NIR spectrophotometer (Agilent, USA) installed at the Center for Polymer and Composite Materials, Hanyang University (Seoul, Republic of Korea). The TEM data of the D_2O/H_2O discriminating nanoprobe (DHDN) were obtained by JEOL JEM 2100F Transmission Electron Microscope installed at the Hanyang LINC3.0 Center for Research Facilities (Seoul, Republic of Korea). The XRD patterns of the DHDN were measured by DB Advance X-ray diffractometer (Bruker Co., USA). A Zetasizer Nano ZSP instrument (Malvern Co., UK) was used to determine the zeta potentials and the size of the DHDN. The Fourier transform infrared (FT-IR) spectra of the DHDN were obtained by using an iS10 Fourier transform infrared spectrophotometer (Thermo Fisher Scientific Co., USA). The photo luminescence emission spectra were recorded using a Flame spectrometer (Ocean Optics, Inc., USA) under external excitation at 808 nm provided by an infrared diode laser (Changchun New Industries Optoelectronics Tech. CO., China). The NIR emission wavelength was selectively measured using 980 nm bandpass filter (Semrock, ff-01–800/12–25, Edmund 980 nm CWL, 12.5 mm Dia., Hard Coated OD 4.0 10 nm), 860 nm bandpass filter, (Thorlabs FBH860–10 Bandpass Filter, Ø25 mm, CWL = 860 nm, FWHM = 10 nm) and NIR camera connected to a mobile device, which was placed on the 3D printed holder.

3. Results and discussion

3.1. Synthesis and characterization of dual-NIR signal emissive DHDNs

To construct a dual-NIR signal-emissive nanoparticle (NP), Nd-Yb co-doped $NaYF_4$ NPs were synthesized using a thermal decomposition synthesis method [21,22]. The $NaYF_4$ crystal structure is regarded as a lattice host material that facilitates efficient energy transfer between co-doped Nd^{3+} and Yb^{3+} ions [23–25]. In Nd-Yb co-doped $NaYF_4$, the Nd^{3+} ions act as both sensitizer and activator ions that absorb and emit irradiation at 808 and 865 nm, respectively. Simultaneously, the energy transferred to the Yb^{3+} ion acts as an activator ion, thus enabling 980 nm emission (Fig. S1).

To achieve a strong luminescence intensity at 980 nm, the optimal concentration of Nd^{3+} was first investigated for $NaYF_4$:Ndx% and Yb5 %. As-synthesized NPs have a spherical morphology and the diameters of Nd15 %, Nd10 %, Nd15 %, Nd17 %, and Nd 20 % were 18.3 ± 1.2, 17.5 ± 2.0, 20.6 ± 2.0, 17.1 ± 1.8, and 18.0 ± 2.0 nm, respectively (Fig. S2a). The X-ray diffraction (XRD) patterns of the $NaYF_4$:x%Nd,5 % Yb NPs were confirmed to have a hexagonal phase, which is well known to be the preferred phase of the host material for efficient luminescence in lanthanide-doped $NaYF_4$ (Fig. S2b) [26–28]. The NIR emission spectrum of $NaYF_4$:x%Nd,5 %Yb was monitored at 865 ($^4F_{3/2} \rightarrow {}^4I_{9/2}$) and 980 nm ($^2F_{5/2} \rightarrow {}^2F_{7/2}$) under 808 nm-laser excitation (Fig. S2c and S2d). As the concentration of Nd^{3+} increases, two competing effects occur: an improved capability for absorbing excitation energy and cross-relaxation-induced luminescence quenching between Nd^{3+} ions. Therefore, the optimal concentration of Nd^{3+} ions was determined to be 17 % based on the brightness optimization of the 980 nm-emission.

Subsequently, further optimization of the Yb^{3+} dopant ions was conducted. TEM images of as-synthesized $NaYF_4$:17 %Nd,y%Yb revealed that their morphology was uniform and spherical, with the average sizes of Yb3 %, Yb5 %, Yb7 %, Yb10 %, and Yb15 % calculated as 16.8 ± 1.4, 17.1 ± 0.9, 21.1 ± 5.6, 18.5 ± 4.3, and 18.8 ± 2.4 nm, respectively (Fig. 2**a**). The XRD patterns revealed that the NP phase of the NPs is consistent with the hexagonal phase (Fig. S3). After optimizing the Nd-Yb co-doped $NaYF_4$, we determined that the optimal concentration with the highest luminescence intensity at 980 nm was $NaYF_4$:Nd17 % and Yb5 %. (Fig. 2**b** and 2**c**).

Finally, the as-synthesized core of the $NaYF_4$:17 %Nd,5 %Yb NP was encapsulated by the inert-$NaYF_4$ shell to minimize surface defects and enhance its optical properties. This encapsulation of $NaYF_4$ could achieve high luminescence intensity while eliminating noise from excitation by using a lower energy source than the core NP. [29,30]. Owing to encapsulation, the size of the $NaYF_4$:Nd17 %Yb5 %@$NaYF_4$ NP, which is a DHDN, increased from 17.1 ± 0.9–23.9 ± 3.2 nm (Fig. S4a). The characteristic absorption of the Nd^{3+} ion peak at approximately 800 nm remained unchanged after encapsulation [31], and the emission intensities increased by approximately 1.45-fold at the detection signal (980 nm) and 1.6-fold at the reference signal (865 nm) (Fig. S4c). The NIR emission intensity of the DHDN showed a substantial spectral overlap with the absorption of H_2O in the 980 nm region, whereas no significant absorption of H_2O was observed near the reference signal of 865 nm (Fig. 2**d**). By contrast, D_2O exhibited no significant absorbance in the NIR region. Therefore, the unique absorption properties of H_2O and D_2O make our proposed dual-NIR emissive DHDN ideal for sensing D_2O at a 980 nm signal with a reference signal in the 865 nm-region.

3.2. NIR optical properties of DHDNs in D_2O and H_2O

The feasibility of the proposed method was examined by evaluating the luminescence properties of the DHDN dispersed in D_2O and H_2O under 808 nm-excitation. To this end, a water-soluble DHDN was prepared via an ionization process using dopamine hydrochloride for practical use in H_2O [7,32,33]. Owing to ionization, FT-IR spectroscopy revealed ligand exchange, as confirmed by the appearance of two new bands at 1608 and 3390 cm^{-1} (Fig. S5a), which were attributed to N–H bending and the stretching of amine groups. [34] Furthermore, zeta potential profiles confirmed the positively charged amine-treated NH_2-NPs after ligand exchange (30.0 mV) (Fig. S5b) [35]. In addition, the absorbance property of the dopamine ligand was compared with DHDN and dopamine hydrochloride dispersed in distilled water (Fig. S6). To assess the stability of the DHDN, they were dispersed in distilled water and stored at 4 °C, while monitoring changes in luminescence intensity and the polydispersity index (PDI) via dynamic light scattering. As shown in Fig. S7, the size and luminescence intensity of the DHDN exhibited negligible change over the one-week observation period.

Owing to water solubilization, the intensity of the detection signal at 980 nm decreased significantly by up to 86 % in H_2O. Conversely, the reference signal at 865 nm showed negligible changes in both D_2O and H_2O (Fig. 3**a**). This notable luminescence quenching at 980 nm suggests its potential for the quantification of D_2O in H_2O, and the stable signal at 865 nm can be used as a good reference signal. As illustrated in Fig. 3**b**, we provide an energy transfer model from the DHDN to H_2O or D_2O. The energy transfer model suggests that energy transfer only to the second overtone of the O–H stretching mode of H_2O is possible. To provide additional evidence of nonradiative energy transfer, we investigated the lifetime properties. As shown in Fig. 3**c**, the lifetime decay of the detection signal was observed at 126.4 μs in D_2O and 43.3 μs in H_2O. This considerable reduction in the lifetime decay of approximately 65.7 % demonstrated their nonradiative energy transfer from Yb^{3+} ions ($^2F_{5/2} \rightarrow {}^2F_{7/2}$) to the O–H vibrations of H_2O ($\nu = 3$) [36]. Inset images of the

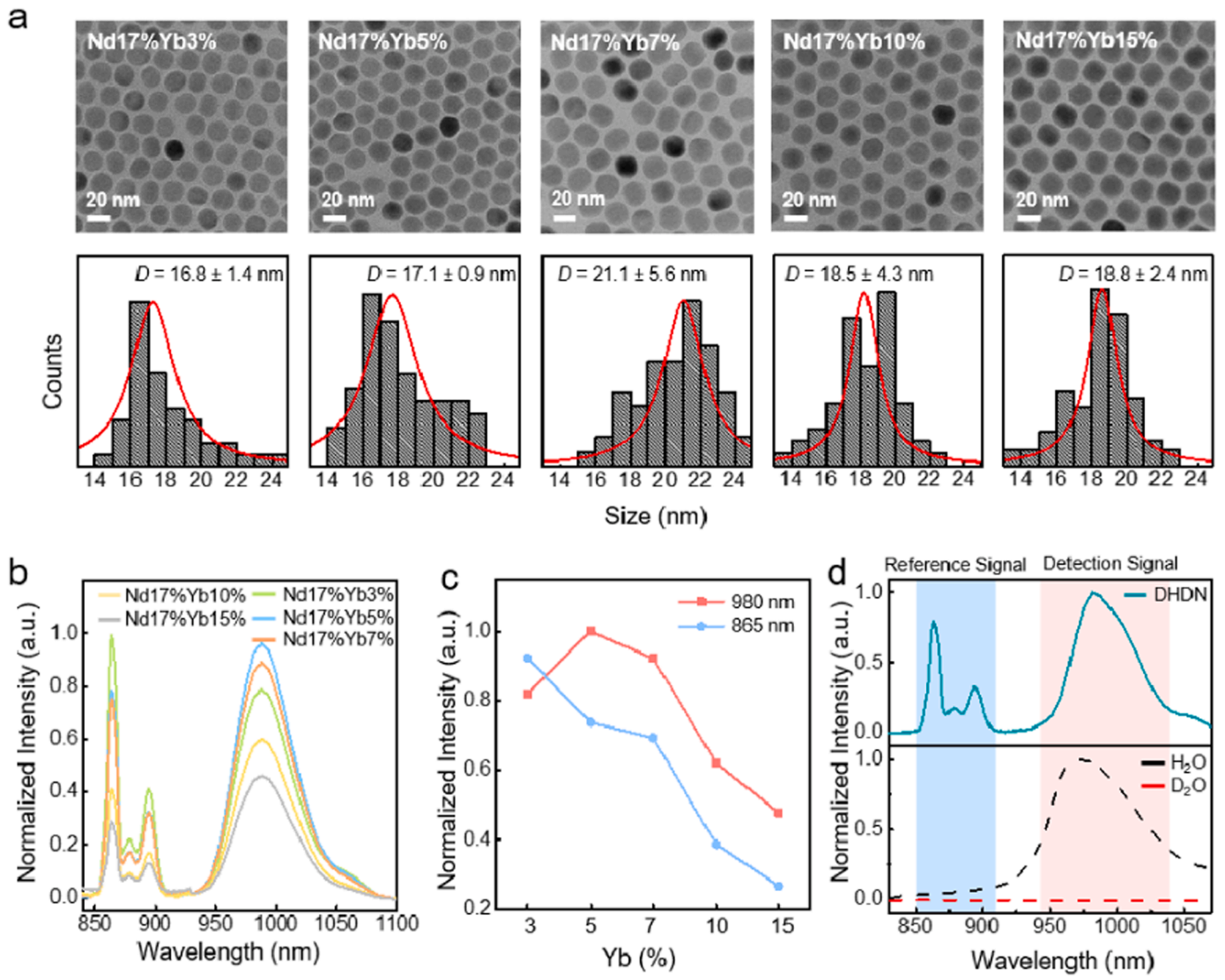

Fig. 2. Characterizations and optimizations of dual-NIR emissive DHDN. (a) TEM images of $NaYF_4$:Nd:17 %,Yb:x%. (b) 865 nm and 980 nm NIR emission spectra of $NaYF_4$:Nd:17 %,Yb:x%. (c) Corresponding intensities of 865 nm and 980 nm NIR emission of $NaYF_4$:Nd:17 %,Yb:x%. (d) Emission spectrum of DHDN in 865 nm and 980 nm with absorption spectra of D_2O and H_2O.

NIR optical image also show the strong attenuation of the 980 nm-emission by H_2O. However, the lifetime of the reference signal confirmed negligible changes in both D_2O and H_2O (45.8 and 46.8 μs, respectively) (Fig. 3**d**). Moreover, we compared the NIR optical images of the DHDN in serially diluted solutions of D_2O and H_2O obtained at 980 and 865 nm, respectively. Optical images were obtained using an NIR camera with a bandpass filter and monitored using a lab-made detection platform (Fig. S8). This portable detection platform comprised an NIR USB camera, USB adapter, bandpass filter, cuvette, 3D printed holder, and smartphone. The NIR emission images from the portable detection platform were captured using a smartphone. The NIR emission intensity of the DHDN at the detection signal decreased as the concentration of D_2O decreased, whereas it remained constant in the reference signal under 808 nm-excitation (Figs. 3**e** and 3**f**). These results indicate that our dual-NIR-emissive DHDN enabled the quantification of D_2O in H_2O and a self-referencing capability.

3.3. Ultrasensitive quantifications of D_2O and H_2O via a dual-NIR emission-based sensing platform

Finally, the ultrasensitive discrimination ability of the developed sensor platform was tested. Mixtures of D_2O/H_2O solutions were subjected to measurements at 980 and 865 nm under 808 nm-excitation using our lab-made sensor platform. The quantification of D_2O in H_2O (Fig. 4**a**) showed that the detection signal increased with increasing concentrations of D_2O (from 0.55 nM to 550 μM). By contrast, the reference signal at 865 nm showed no obvious changes with increasing concentrations of D_2O. The corresponding calibration curves (detection signal/reference signal) are shown in Fig. 4**b**, exhibiting a relatively high coefficient of determination ($R^2 = 0.99$), with the LOD calculated as 0.17 nM.

Given our success in quantification, we further tested the performance of D_2O sensing in various H_2O-based solutions, including a PBS buffer, HEPES buffer, diluted Rose Bengal solution, and diluted methylene blue solution. The most used buffer solutions in biological experiments and colored stain were chosen. In conventional D_2O sensors, these salt buffer solutions can affect the performance of the D_2O sensor during operation. In addition, optical-based D_2O sensors, which rely on visible emissions, are not available for these various colored solutions because they can affect the color of the samples being analyzed, thus causing noise. Our proposed approach utilizes NIR absorption and emission, thus demonstrating its potential for successful detection in both buffer and

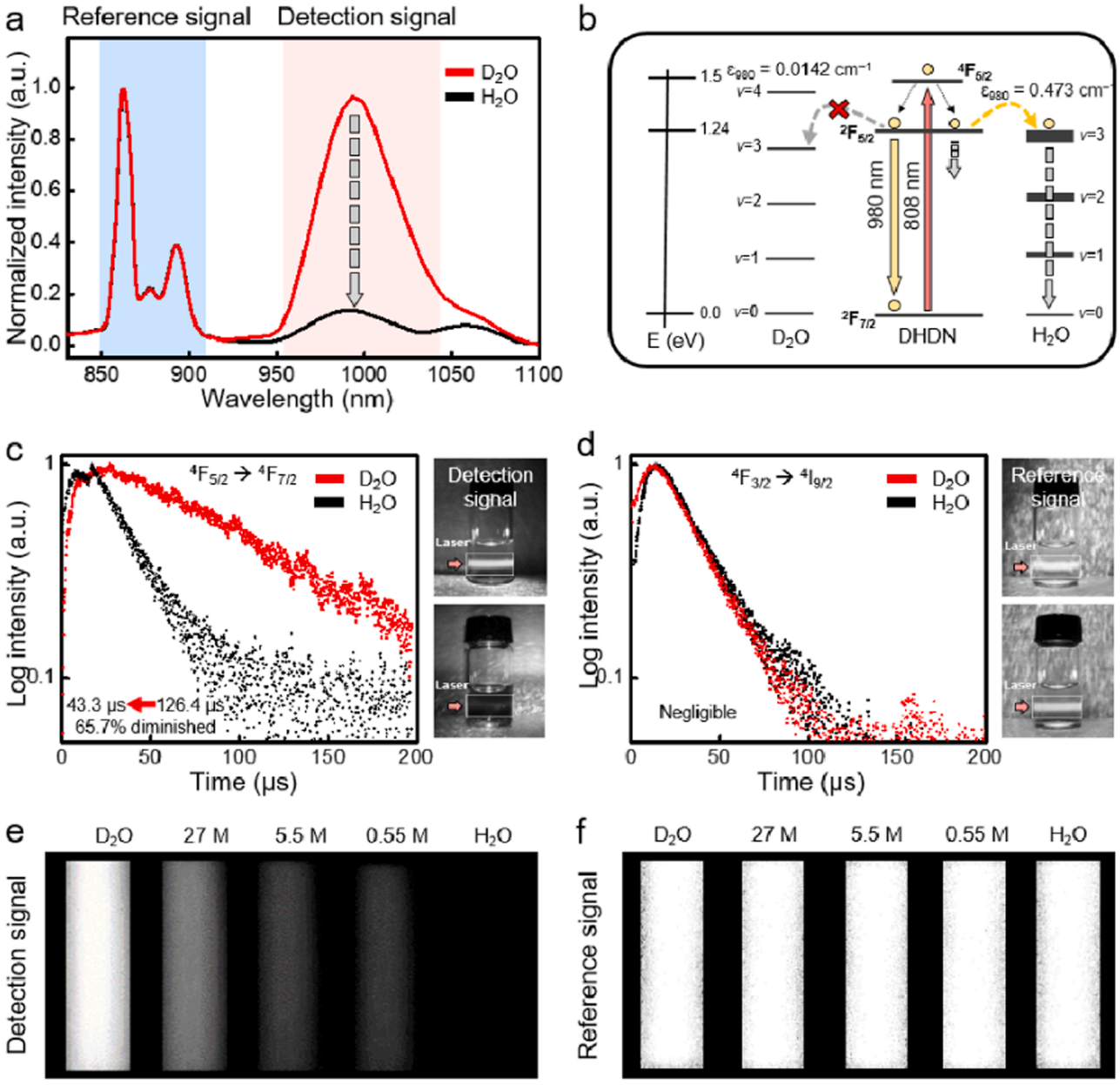

Fig. 3. Characterizations of DHDN in D_2O and H_2O. (a) NIR emission spectra of DHDN dispersed in D_2O and H_2O, respectively. (b) Schematic illustrations of the energy transfer from DHDN to D_2O and H_2O in D_2O or H_2O. (c) Time decay measurement profile of DHDN in D_2O and H_2O at 980 nm-emission. (d) Time decay measurement profile of DHDN in D_2O and H_2O at 865 nm-emission. (e) 980 nm-luminescence images of different concentrations of D_2O solutions under 808 nm excitation. (f) 865 nm-luminescence images of different concentrations of D_2O solutions under 808 nm excitation.

colored solutions. To demonstrate this, the absorption properties of various solutions were monitored (Fig. 4**c**). These absorption properties in the NIR region were solely due to H_2O, thus suggesting that the various solutions were independent in these NIR regions. Next, we evaluated the changes in the detection and reference signals in a 10 % D_2O diluted solution. Fig. 4**d** shows that the emission intensity remains stable in pure H_2O, various buffer solutions, and diluted dyes, thus demonstrating that the presence of salts or dyes in these solutions does not affect the signal intensity. This minor fluctuation indicates that the proposed D_2O sensing method is highly applicable for practical H_2O-based solutions. To compare these results with those of other optical-based D_2O sensors, the LOD and operation types of other sensors reported in literature are summarized in Table S1. These results highlight the remarkable sensing performance of our sensor platform with an LOD of 0.17 nM, which is the most sensitive D_2O sensing approach to date. Therefore, we report that our developed sensor platform is capable of accurate measurements and ultrasensitive discrimination between D_2O and H_2O.

4. Conclusions

We demonstrated a self-referenced dual-NIR emission-based D_2O sensing platform. The developed DHDN was optimized to emit strong emission intensities at 980 and 865 nm as the D_2O detection and reference signals, respectively. Owing to the strong absorption of H_2O based on a specific wavelength of 980 nm, our D_2O sensor platform exhibited outstanding performance with an ultrasensitive LOD of 0.17 nM for D_2O. To the best of our knowledge, this study represents the most sensitive D_2O sensor platform compared with previously reported D_2O sensors. Furthermore, the reference signal at 865 nm offered a

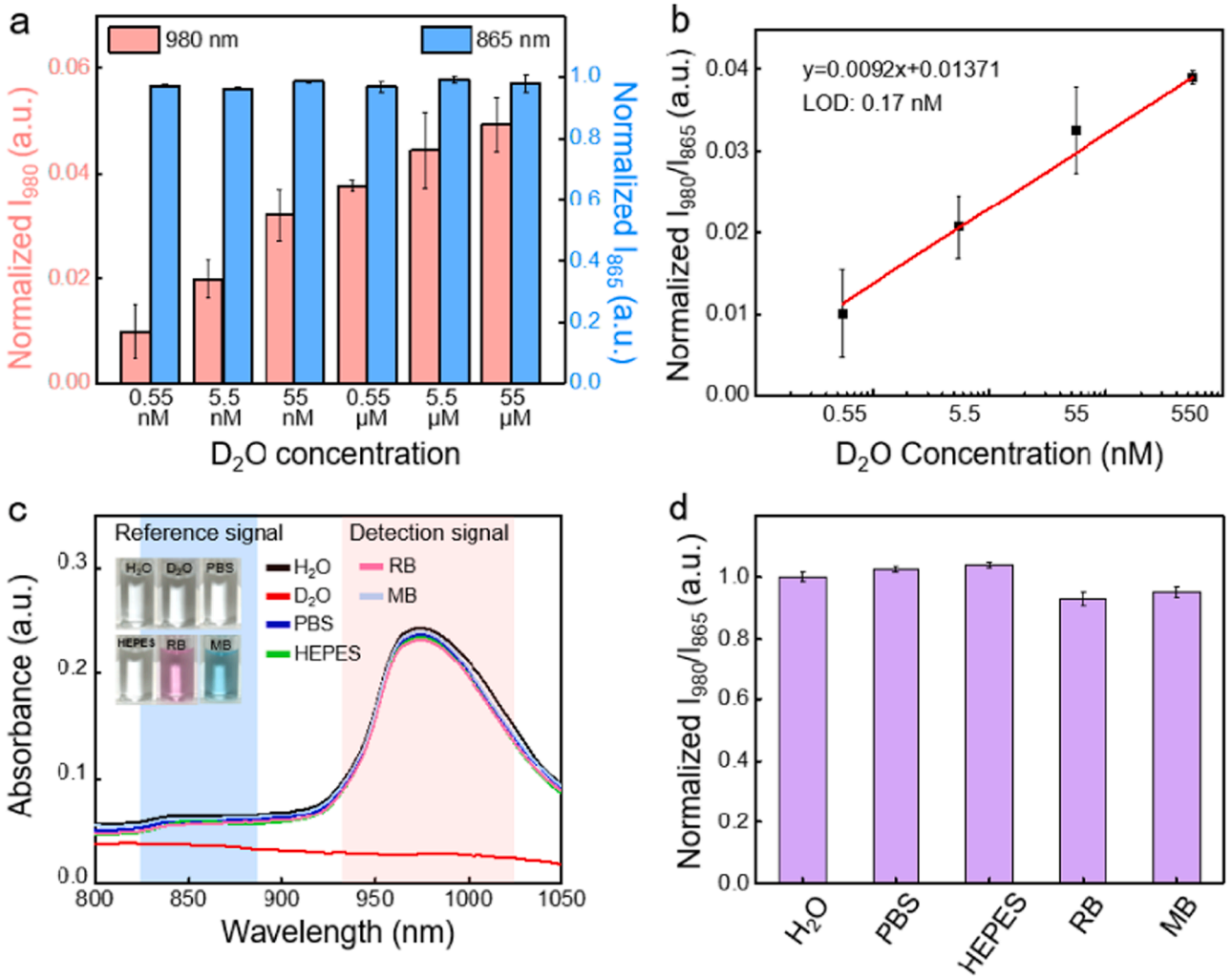

Fig. 4. Quantifications of D_2O/H_2O using developed sensing platform. (a) NIR emission intensities in serially diluted D_2O solutions. 980 nm emission (red bar) and 865 nm emission (blue bar) (b) Calibration curve of normalized emission intensity (I_{980}/I_{865}, Emission intensity at 980 nm/865 nm). (c) Absorbance spectrum of PBS, HEPES, diluted rose bengal and diluted methylene blue. (Inset: optical images of various solutions) (d) Relative emission intensity at I_{980}/I_{865} upon addition of 10 % D_2O in various solutions (PBS, HEPES, diluted rose bengal and diluted methylene blue). All experiments were conducted under room temperature.

stable signal intensity in both D_2O and H_2O. Thus, our D_2O sensor platform demonstrated high sensitivity and an accurate D_2O detection process. In addition, the advantages of this NIR region provided a sensor platform that could be used for practical H_2O-based buffer solutions, including PBS, HEPES, and various colored solutions. This study provides the first report of a detection method for D_2O in the NIR region and has great potential for further applications in fields that require the ultrasensitive discrimination of D_2O and H_2O.

CRediT authorship contribution statement

Dongkyu Kang: conceptualization, investigation, methodology, formal analysis, writing – original draft. **Eunjin Park**: investigation, methodology, formal analysis, writing – original draft. **Kayoung Kim**: investigation, formal analysis. **Joonseok Lee**: conceptualization, supervision, writing - review & editing, funding acquisition.

Declaration of Competing Interest

The authors declare the following financial interests/personal relationships which may be considered as potential competing interests: Joonseok Lee reports financial support was provided by Ministry of Science and ICT.

Data availability

Data will be made available on request.

Acknowledgements

This research was supported by the National Research Foundation of Korea (NRF) grant funded by the Korea government (MSIT) (NRF-2021M3E5E3080381, NRF-2023R1A2C2003128).

Appendix A. Supporting information

Supplementary data associated with this article can be found in the online version at doi:10.1016/j.snb.2023.134948.

References

[1] S. Gadiyaram, P. Kumar, A. Singh, D.A. Jose, Detection and discrimination of water (H_2O) and heavy water (D_2O) by an off-the-shelf fluorescent probe, Microchem. J. 176 (2022), 107244.
[2] Z. Han, J. Wang, P. Du, J. Chen, S. Huo, H. Guo, et al., Highly facile strategy for detecting D_2O in H_2O by porphyrin-based luminescent probes, Anal. Chem. 94 (2022) 8426–8432.
[3] S.G. Dunning, A.J. Nuñez, M.D. Moore, A. Steiner, V.M. Lynch, J.L. Sessler, et al., A sensor for trace H_2O detection in D_2O, Chem 2 (2017) 579–589.

[4] Y.J. Luo, C. Li, W.C. Zhu, X.J. Zheng, Y. Huang, Z.Y. Lu, A facile strategy for the construction of purely organic optical sensors capable of distinguishing D_2O from H_2O, Angew. Chem. Int. Ed. 58 (2019) 6280–6284.
[5] B. Dong, Y. Lu, W. Song, X. Kong, Y. Sun, W. Lin, A dual-site controlled fluorescent sensor for the facile and fast detection of H_2O in D_2O by two turn-on emission signals, Chem. Commun. 56 (2020) 1191–1194.
[6] D.H. Ortgies, M. Tan, E.C. Ximendes, B. Del Rosal, J. Hu, L. Xu, et al., Lifetime-encoded infrared-emitting nanoparticles for in vivo multiplexed imaging, ACS Nano 12 (2018) 4362–4368.
[7] D. Kang, H.J. Ahn, J. Lee, S.K. Kim, J. Pyun, C.S. Song, et al., An NIR dual-emitting/absorbing inorganic compact pair: a self-calibrating LRET system for homogeneous virus detection, Biosens. Bioelectron. 190 (2021), 113369.
[8] J.M. Lim, M. Supianto, T.Y. Kim, B.S. Kim, J.W. Park, H.H. Jang, et al., Fluorescent lateral flow assay with carbon nanodot conjugates for carcinoembryonic antigen, Biochip J. 17 (2023) 93–103.
[9] J.J. Max, C. Chapados, Isotope effects in liquid water by infrared spectroscopy. III·H_2O and D_2O spectra from 6000 to 0 cm^{-1}, J. Chem. Phys. 131 (2009), 184505.
[10] M.R. Lacroix, Y. Liu, S.H. Strauss, Room-temperature FTIR spectra of the cyclic S(4) (H(2)O)(4) cluster in crystalline $Li_2(H_2O)_4(B_{12}F_{12})$: observation of B and E ν(OH) bands and coupling of strong O-H.O and weak O-H.F vibrations, J. Phys. Chem. A 123 (2019) 9781–9790.
[11] Q. Su, W. Feng, D. Yang, F. Li, Resonance energy transfer in upconversion nanoplatforms for selective biodetection, Acc. Chem. Res. 50 (2017) 32–40.
[12] J. Maillard, K. Klehs, C. Rumble, E. Vauthey, M. Heilemann, A. Furstenberg, Universal quenching of common fluorescent probes by water and alcohols, Chem. Sci. 12 (2020) 1352–1362.
[13] S. Kim, S. Ryoo, E.K. Park, S.H. Cha, H.S. Song, K. Kim, et al., On-site remote monitoring system with NIR signal-based detection of infectious disease virus in opaque salivary samples, ACS Sens 8 (2023) 1299–1307.
[14] L. Bishwal, S. Kar, S. Bhattacharyya, Role of noncovalent interactions in N,P-functionalized luminescent carbon dots for ultrasensitive detection of moisture in D_2O: boosting visible-NIR light sensitivity, ACS Appl. Mater. Interfaces 15 (2023) 15907–15916.
[15] R.X. Ji, J.S. Shen, Modulating dual fluorescence emissions in imine-based probes to distinguish D_2O and H_2O, J. Phys. Chem. B. 127 (2023) 1229–1236.
[16] Y. Sun, H. Jin, X. Jiang, R. Gui, Assembly of black phosphorus nanosheets and MOF to form functional hybrid thin-film for precise protein capture, dual-signal and intrinsic self-calibration sensing of specific cancer-derived exosomes, Anal. Chem. 92 (2020) 2866–2875.
[17] Y. Zhang, B. Yan, A portable self-calibrating logic detector for gradient detection of formaldehyde based on luminescent metal organic frameworks, J. Mater. Chem. C 7 (2019) 5652–5657.
[18] L. Tan, H. Ding, S. Chanmungkalakul, L. Peng, G. Yuan, Q. Yang, et al., A smart TP-FRET-based ratiometric fluorescent sensor for bisulfite/formaldehyde detection and its imaging application, Sens. Actuators B 345 (2021), 130331.
[19] W. Mi, T. Shen, X. Guo, X. Liu, M. Zhang, M. Jia, Ratiometric quantification and visual detection of sulfur dioxide residues using a coumarin-derived fluorescent probe, Sens. Actuators B 395 (2023), 134459.
[20] L. Liang, J. Chen, K. Shao, X. Qin, Z. Pan, X. Liu, Controlling persistent luminescence in nanocrystalline phosphors, Nat. Mater. 22 (2023) 289–304.
[21] F.J. Pedraza, C. Rightsell, G.A. Kumar, J. Giuliani, C. Monton, D.K. Sardar, Emission enhancement through Nd^{3+}-Yb^{3+} energy transfer in multifunctional $NaGdF_4$ nanocrystals, Appl. Phys. Lett. 110 (2017), 223107.
[22] J.C. Boyer, L.A. Cuccia, J.A. Capobianco, Synthesis of colloidal upconverting $NaYF_4$: Er^{3+}/Yb^{3+} and Tm^{3+}/Yb^{3+} monodisperse nanocrystals, Nano Lett. 7 (2007) 847–852.
[23] K.A. Abel, J.C. Boyer, F.C.J.M. van Veggel, Hard proof of the $NaYF_4/NaGdF_4$ nanocrystal core/shell structure, J. Am. Chem. Soc. 131 (2009) 14644–14645.
[24] B.S. Cao, Y.N. Bao, Y. Liu, J.Y. Shang, Z.Y. Zhang, Y.Y. He, et al., Wide-range and highly-sensitive optical thermometers based on the temperature-dependent energy transfer from Er to Nd in Er/Yb/Nd codoped $NaYF_4$ upconversion nanocrystals, Chem. Eng. J. 385 (2020), 123906.
[25] D. Kang, H.S. Kim, S. Han, Y. Lee, Y.-P. Kim, D.Y. Lee, et al., A local water molecular-heating strategy for near-infrared long-lifetime imaging-guided photothermal therapy of glioblastoma, Nat. Commun. 14 (2023), 2755.
[26] F. Wang, Y. Han, C.S. Lim, Y.H. Lu, J. Wang, J. Xu, et al., Simultaneous phase and size control of upconversion nanocrystals through lanthanide doping, Nature 463 (2010) 1061–1065.
[27] H.S. Qian, Y. Zhang, Synthesis of hexagonal-phase core-shell $NaYF_4$ nanocrystals with tunable upconversion fluorescence, Langmuir 24 (2008) 12123–12125.
[28] S. Liu, Z. An, B. Zhou, Optical multiplexing of upconversion in nanoparticles towards emerging applications, Chem. Eng. J. 452 (2023), 139649.
[29] Y. Zhang, P. Lei, X. Zhu, Y. Zhang, Full shell coating or cation exchange enhances luminescence, Nat. Commun. 12 (2021), 6178.
[30] D. Kang, S. Lee, H. Shin, J. Pyun, J. Lee, An efficient NIR-to-NIR signal-based LRET system for homogeneous competitive immunoassay, Biosens. Bioelectron. 150 (2020), 111921.
[31] Y. Zhong, G. Tian, Z. Gu, Y. Yang, L. Gu, Y. Zhao, et al., Elimination of photon quenching by a transition layer to fabricate a quenching-shield sandwich structure for 800 nm excited upconversion luminescence of Nd^{3+}-sensitized nanoparticles, Adv. Mater. 26 (2014) 2831–2837.
[32] S.F. Himmelstoß, T. Hirsch, Long-term colloidal and chemical stability in aqueous media of $NaYF_4$-type upconversion nanoparticles modified by ligand-exchange, Part. Part. Syst. Charact. 36 (2019), 1900235.
[33] M.J. Byun, J. Lim, S.-N. Kim, D.-H. Park, T.-H. Kim, W. Park, et al., Advances in nanoparticles for effective delivery of RNA therapeutics, Biochip J. 16 (2022) 128–145.
[34] H. Hu, L. Xiong, J. Zhou, F. Li, T. Cao, C. Huang, Multimodal-luminescence core-shell nanocomposites for targeted imaging of tumor cells, Chem. Eur. J. 15 (2009) 3577–3584.
[35] M.C. Gruner, M.S. Arai, M. Carreira, N. Inada, A.S.S. de Camargo, Functionalizing the mesoporous silica shell of upconversion nanoparticles to enhance bacterial targeting and killing via photosensitizer-induced antimicrobial photodynamic therapy, ACS Appl. Bio Mater. 1 (2018) 1028–1036.
[36] R. Arppe, I. Hyppänen, N. Perälä, R. Peltomaa, M. Kaiser, C. Würth, et al., Quenching of the upconversion luminescence of $NaYF_4$: Yb^{3+}, Er^{3+} and $NaYF_4$: Yb^{3+}, Tm^{3+} nanophosphors by water: the role of the sensitizer Yb^{3+} in non-radiative relaxation, Nanoscale 7 (2015) 11746–11757.

Dongkyu Kang has received his B.S. degree from the department of Systems Biotechnology at Chung-Ang University, South Korea. Currently, He is a Ph.D. candidate in department of chemistry at Hanyang University. Now his scientific interests lie in the field of lanthanide-doped nanomaterials with various applications such as biosensor, healthcare and their optical phenomena.

Eunjin Park received her B.S. degree from the Department of Chemistry at Hanyang University, South Korea. Currently, she is a M.S. candidate in the Department of Chemistry, Hanyang University. Currently, her research interests lie in the developments and applications of lanthanide nanoparticles.

Kayoung Kim received a B.S. degree (2011) in Materials Science and Engineering from Pohang University of Science and Technology (POSTECH) and a Ph.D. degree (2020) in Materials Science and Engineering from Korea Advanced Institute of Science and Technology (KAIST), Republic of Korea. Currently, she is an assistant professor at the Dankook University. Her research interests are the rational design of functional nanomaterials and (photo)electrochemical sensing platforms.

Joonseok Lee has received his B.S. degree from the department of Material Science and Engineering, Hanyang University, South Korea and the Ph.D. degree from the department of Materials Sciences, Korea Advanced Institute of Science and Technology (KAIST), South Korea. He held a post-doctoral position at the Argonne National Laboratory, Lemont, IL, USA, where he was involved in the Center for Nanoscale Materials. He is now an Associate Professor at the department of chemistry, Hanyang University, South Korea. His research interests focus on the engineering and characterizations of various functional nanomaterials such as lanthanide-doped nanomaterials, silica nanostructures, and various inorganic nanomaterials. The applications include biosensors, healthcare, energy, and environments.